



ORIGINAL RESEARCH ARTICLE

Investigation and Feasibility of Printing Polyoxymethylene Semi-crystalline Polymer Parts with Fused Filament Fabrication 3D Printer and Evaluation of Mechanical Properties of the Printed Samples

Behnam Akhoundi  and Vahid Modanloo

Submitted: 21 May 2023 / Accepted: 4 August 2023

Fused filament fabrication (FFF) is one of the simple and cost-efficient methods of additive manufacturing (AM) of complex objects which has widespread applications in various industries. Developing 3D printing materials is one of the main challenges that scientists are dealing with in this method. Currently, the materials used for 3D printing are amorphous polymers and semi-crystalline polymers that behave similarly to amorphous polymers in the melting process. This is because of the less shrinkage of amorphous thermoplastic materials compared to semi-crystalline polymers which facilitate printing. Since semi-crystalline polymers exhibit better mechanical characteristics compared to amorphous polymers, these materials must be used in the FFF process as well. However, it must be noted that printing these materials is difficult as they show high shrinkage. Particularly, this can be seen by the weak adhesion of the first layer to the bed and the layers' adhesion to each other as a result of high shrinkage. Therefore, this paper aims to assess the feasibility of printing objects from semi-crystalline polymers made of polyoxymethylene (POM). The parameters under study include raster angle, nozzle temperature, filling pattern, filling percentage, and fan mode. The experiments showed that due to high shrinkage, it is not possible to print semi-crystalline parts the same as the parts made of amorphous polymers. However, these parts can be printed by changing the printing direction. Moreover, it is observed that under a specified direction, without the fan, low nozzle temperature, low filling percentage, and 0/90 filling pattern, the semi-crystalline parts are printed more easily. Finally, the mechanical properties of the standard printed samples were evaluated, and the maximum tensile strength, flexural strength, and compressive strength are 11.5, 28, and 8 MPa, respectively.

Keywords 3D printer, additive manufacturing, fused filament fabrication, polyoxymethylene (POM), semi-crystalline polymers, shrinkage

1. Introduction

Additive manufacturing (AM) methods are used in various industries for the production of conceptual models, rapid prototyping and even functional parts (Ref 1). Generally, in AM, the three-dimensional (3D) model is sliced into two-dimensional layers and will be printed layer-by-layer (Ref 2, 3). Due to the essence of the manufacturing process in AM, it is possible to produce a part with a complex geometry without the need for jigs and fixtures, and additional tools, by reducing manufacturing's time and cost (Ref 4). Among AM methods, the fused filament fabrication (FFF) method has been more developed due to its simplicity and cheapness (Ref 5, 6). In the FFF process, the thermoplastic filament is melted and then extruded through a nozzle. Acrylonitrile butadiene styrene

(ABS) (Ref 7), polylactic acid (PLA), high impact polystyrene (HIPS) (Ref 7), polycarbonate (PC) (Ref 7), polypropylene (PP) (Ref 8), polyether ether ketone (PEEK) (Ref 9), polyetherimide (PEI) (Ref 10), polyethylene terephthalate glycol (PETG) (Ref 11), polyamide (PA) (Ref 12), polyethylene (LDPE, HDPE) (Ref 13), Poly(methyl methacrylate) (PMMA) (Ref 14), polycaprolactone (PCL) (Ref 15), polyoxymethylene (POM) (Ref 16), etc. are some of the neat thermoplastic polymer materials that have been used in the FFF process. Thermoplastic materials are divided into two categories: semi-crystalline and amorphous materials (Ref 17). A shrinkage phenomenon occurs in the cooling cycle in both categories but the amount of shrinkage is extremely high in semi-crystalline polymer materials (Ref 18). Shrinkage in the FFF process can affect the dimensional accuracy of the part as well as deformation of the printed part in the form of warpage, delamination, cracking, damage to the created supports, and even cause the part to be unprintable (Ref 19). The FFF process is simple and it is possible to print complex parts. However, the surface quality, dimensional accuracy, and mechanical and thermal properties of the parts printed by this process are highly dependent on printing parameters such as nozzle temperature, ambient temperature, bed or substrate temperature, layer height, nozzle diameter, extrusion width, air gap, build direction, part orientation, raster angle, filling pattern, filling percentage, printing speed, and filament material (Ref 20). Therefore, much

Behnam Akhoundi and Vahid Modanloo, Department of Mechanical Engineering, Sirjan University of Technology, Sirjan, Kerman Province, Iran. Contact e-mail: b.akhoundi@sirjantech.ac.ir.

research has been conducted on the effect of these parameters on the various properties of the printed product (Ref 21, 22). Also, extensive research has been done to improve the mechanical properties of printed products by improving the mechanical properties of the used materials (Ref 23). In this context, it is possible to mention the addition of fillers (metal particles, chopped glass, and carbon fibers) (Ref 24-28), nanomaterial (Ref 26), heat treatment after the process (Ref 29), using ultrasonic waves (Ref 30, 31), etc. Also, extensive research has been done on the use of continuous fibers (glass, carbon, and Kevlar) to strengthen the printed parts (Ref 32-35). On the other hand, less research has been done on printing parts with widely used semi-crystalline materials such as PE, PP, and POM.

Generally, in the FDM process, the “bed or substrate” consists of glass or metal materials coated with some type of adhesive (glue). A critical problem for semi-crystalline printing in FFF 3D printing is the lack of adhesion between the thermoplastic materials on this substrate. Initial attempts were made to print PE onto substrates at different temperatures, resulting in poor adhesion (Ref 25). Alternatively, Nabipour et al. (Ref 25) used a thin sheet of PP as a bed for printing PE-based composites. PP is a semi-crystalline thermoplastic with the most similar properties to PE but with a higher melting point, which served as a coating on the bed to supposedly allow the adhesion of the molten PE material to the substrate (Ref 24, 25).

PP used in the production of various parts with good mechanical properties and low production costs. Carneiro et al. (Ref 8) evaluated the influence of the parameters such as raster orientation, layer height, and infill percentage on the mechanical properties of neat PP and glass-fiber-reinforced PP. Zhang and Gao (Ref 36) improved the printability of PP random copolymer by adding short glass fibers and ethylene propylene diene monomer. Polyakov et al. (Ref 37) investigated the biocompatibility of high-performance semi-crystalline polyimide samples printed via an FFF 3D printer.

POM is an engineering thermoplastic that has exclusive properties such as low friction and high impact resistance (Ref 38). POM is commonly used in various industrial applications such as gears and bearings. It also has high rigidity, excellent wear resistance, good chemical resistance, etc. However, POM has usually processed by injection molding and extrusion methods. The potential for using POM for parts fabricated with FFF is significant for both industrial applications and niche prototyping needs, but to date, this has received little attention in the literature (Ref 38). Muro-Fraguas et al. (Ref 39) used an atmospheric pressure air plasma treatment to a polycarbonate (PC)-printing base for increasing the adhesion of POM to the PC base. The results show an increase in adhesion of up to 45% is achieved. Wang and Yeh (Ref 40) printed POM samples successfully and stated that the raster orientation has a great influence on the tensile strength of specimens. Lebedev et al. (Ref 41) investigated thermophysical, rheological and morphological properties of carbon nanotube/POM composite for usage in AM. Tian (Ref 38) characterized the 3D-printed POM samples in order to investigate the impact of infill direction on elastic, viscoelastic, and shear properties. In this work, ABS glue (solved ABS in Aston) was used between the samples being printed and the build plate. Akhouni et al. (Ref 11) succeeded in the printing of POM/Continuous glass fiber composite material and evaluated its mechanical properties. They also stated that by using the neat POM filament, problems

were raised due to the high shrinkage of neat POM and the desirable part could not be printed.

As stated before, the bulk of studies investigated amorphous polymers, and less attention has been paid to the development of semi-crystalline polymers for printing. Therefore, this study aims to assess the feasibility of printing parts from semi-crystalline POM polymers which exhibit high shrinkage compared to amorphous polymers and it is troublesome to print parts using these materials. To do so, the effects of five parameters, i.e., the raster angle, nozzle temperature, filling pattern, filling percentage, and the fan mode (off, on) on the feasibility of printing parts are studied by heat transfer viewpoint.

2. Amorphous and Semi-crystalline Polymer Materials

Thermoplastic polymers have long molecular chains that are aligned together by weak van der Waals intermolecular forces (Ref 17). When these materials are affected by heat, their intermolecular forces weaken and make them soft and flexible, and finally melt when the heat goes beyond a certain temperature. Thermoplastic polymers were categorized into two groups: amorphous and semi-crystalline (Ref 42). Table 1 shows a general comparison of the properties of semi-crystalline and amorphous polymeric materials. In general, it can be said that semi-crystalline polymers have more advantages for mechanical applications compared to amorphous polymers.

One of the main differences between amorphous and semi-crystalline polymers is the amount of shrinkage of these. Amorphous polymers exhibit a slight volume change during solidification due to their irregular structure; meanwhile, semi-crystalline polymers have a greater reduction in volume due to the formation of a semi-crystalline structure (Ref 17, 43). The typical volume reduction of amorphous and semi-crystalline polymers is shown in Fig. 1.

The FFF process is one of the simple processes for manufacturing complex parts made of polymers (Ref 44). Generally, amorphous polymers are used for printing parts due to low shrinkage. Due to the advantages of semi-crystalline materials in comparison to amorphous materials, it is necessary to use this type of polymer in the FFF process. Figure 2 shows a printed cubic piece made of amorphous and semi-crystalline polymer. As can be seen, it is not possible to print parts with semi-crystalline polymer (with the same printing conditions for both types of materials). The main reason for this is the high shrinkage percentage of semi-crystalline polymers.

Table 1 general characteristic of amorphous and semi-crystalline polymers

Amorphous polymers	Semi-crystalline polymers
Without melting point (glass transition)	With melting point
Usually transparent	Usually opaque
Low shrinkage	High shrinkage
Low chemical resistance	High chemical resistance
Low wear and fatigue resistance	High wear and fatigue resistance

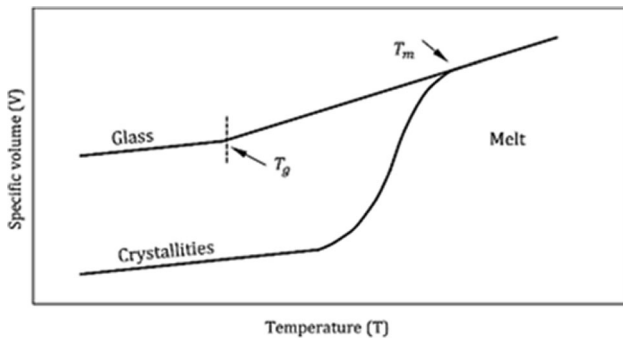


Fig. 1 Shrinkage in amorphous and semi-crystalline polymers

Parameters	PLA	POM
T = 210°C Part Fill Style = ±45 Fill Density = 30% Fan = ON		
T = 225°C Part Fill Style = ±45 Fill Density = 30% Fan = ON		
T = 225°C Part Fill Style = ±45 Fill Density = 100% Fan = ON		

Fig. 2 Rectangular cubic printed parts with the amorphous (PLA) and semi-crystalline polymers (POM): (a) low nozzle temperature and fill percentage, (b) high nozzle temperature and low fill percentage, and (c) high nozzle temperature and fill percentage

3. Materials, Methods, and Equipment

POM filament with a diameter of 1.75 mm purchased from Gizmo Dorks Company was used as feedstock, 3D printer Quantum 2020 (Iran) with table dimensions of 195 x 195 x 200 was used to print samples, and Simplify 3D software was used to slice and generate G-code. The used FFF printer has a blower fan for better sample cooling, and the fan speed can be set up to 255 rpm. To check the tensile, flexural, and compressive mechanical properties, the samples are printed according to ASTM D638 type 4, ASTM D790, and ASTM D695 standards, respectively, and mechanical tests are performed using the SANTAM-20 (Tehran, Iran) device with a load capacity of 20 KN. For all tests, five samples were printed from each standard sample and the average of the results was reported.

4. Design of Experiment to Examine the Possibility of Printing Semi-crystalline Parts

A rectangular cubic part with dimensions of 20 x 20 x 10 mm was selected to investigate the feasibility of printing this part with POM using the FFF process. Since the shrinkage of semi-crystalline polymers has a direct relationship with the percentage of crystallization, therefore, the parameters were selected to study the feasibility of printing the part, which is related to the crystallization structure of the part. One of the important parameters that affect the crystallization percentage is the cooling rate of the printing part. Therefore, the parameters of nozzle temperature, filling percentage, fan modes, filling pattern, and printing direction of the part were selected as investigation parameters. Figure 3 shows the selected directions for printing the part and the filling pattern. The purpose of modes II and III is to reduce the contact surface and, as a result, reduce the cooling rate. It should be noted that in the tests when the fan is on, the fan starts working from the third layer in all experiments. The considered levels for the parameters are given in Table 2. 114 experiments were done with these levels of parameters and with three-time repeats in each experiment. Also, constant process parameters are shown in Table 3.

5. Results and Discussion

The performed experiments (printed samples) are shown in Fig. 4(a), (b), and (c). As can be seen, by changing the printing direction, the possibility of printing semi-crystalline parts provided that the process parameters are selected correctly, increases. The results of the experiments will be discussed in the following.

5.1 Printing Direction of Parts

As mentioned in Sect. 2, the shrinkage of semi-crystalline polymer materials has a direct relationship with the cooling rate. As a result, it is very important to investigate the heat transfer of the deposited rasters. Figure 5 shows the heat transfer in the rasters of the first and secondary layers. It is assumed that (q_1) is the convection heat transfer of the environment and the rasters, (q_2) is the conduction heat transfer between the raster and the raster, and (q_3) is the conduction heat transfer of the rasters and the printer bed. The total heat transferred from the raster to the ambient environment in the first layer and second layers are determined according to Eq 1 and 2 (Ref 45):

$$\dot{Q}_1 = \dot{q}_1 + \dot{q}_2 + \dot{q}_1 \quad (\text{Eq 1})$$

$$\dot{Q}_n = \dot{q}_1 + 2\dot{q}_2 \quad (\text{Eq 2})$$

where \dot{Q}_1 and \dot{Q}_n are the heat transfer of the rasters placed in the first layer and the nth layer, respectively. Since the heat transfer that occurred between the raster and the raster is less than the raster and the bed ($q_2 < q_3$), it can be concluded that the heat transfer of the raster in the first layer is more than the next layers. As a result, the rate of shrinkage amount in the first layer is higher than in the next layers. This shows that the initial layers are of great importance and the process parameters should be selected in such a way that the shrinkage in the first

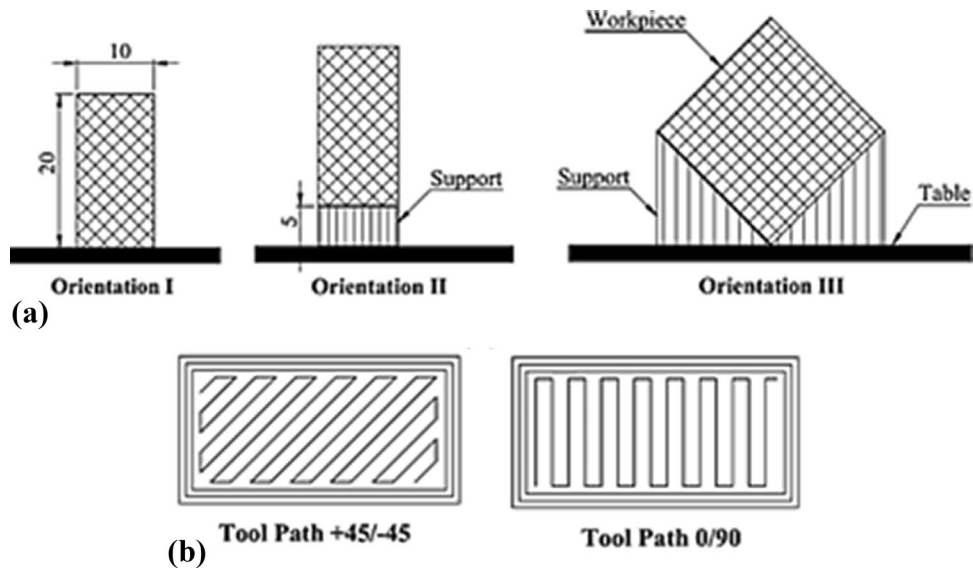


Fig. 3 Printing orientation and printing patterns: (a) three printing orientation and (b) two filling printing patterns

Table 2 Levels of investigation parameters

Parameters	Levels
Temperature, °C	210-225
Fill percentage, %	30-100
Filling pattern	± 45-0/90
Fan mode	On/Off
Built orientation	I, II, and III

Table 3 Constant parameters in printing process

Parameters	Levels
Dimension of 3D printing bed, mm	195 × 195 mm
Printing speed, mm/s	30
Bed temperature, °C	90
Number of counters	3
Fan speed	127
Nozzle diameter, mm	0.4
Layer height, mm	0.02

layer is reduced and the semi-crystalline part can be printed. Assuming that the material is elastic can be concluded from the relationship between strain and expansion of the material (Eq 3) (Ref 46) and the relationship between stress and strain (Eq 4) and (Eq 5) (Ref 46):

$$\varepsilon = \alpha \Delta T \quad (\text{Eq } 3)$$

$$\sigma = E\varepsilon \quad (\text{Eq } 4)$$

$$F = AE\alpha\Delta T \quad (\text{Eq } 5)$$

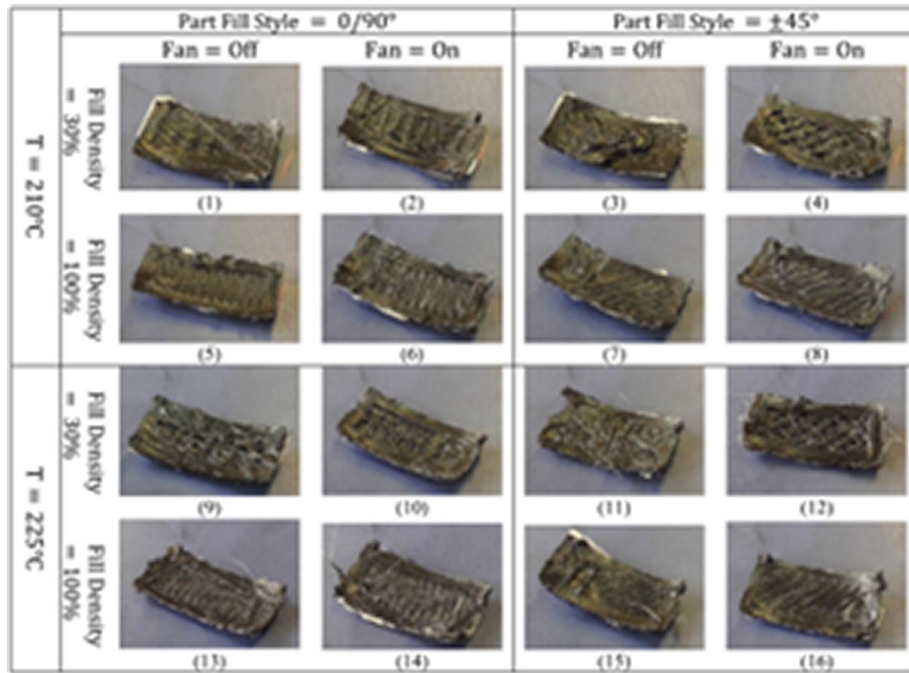
where ε is the strain, α is the expansion coefficient, ΔT is the temperature change, E is the elastic modulus, σ is the stress, A is the cross-sectional area of raster and F is the force produced by material shrinkage. According to Eq 5, it can be concluded that a large decrease in temperature or high heat transfer causes more force, and if this force is greater than the adhesive force of

between the raster and the table or between the raster and the raster, it causes the deposited layer to be plunked from the printer table or from the previous layer.

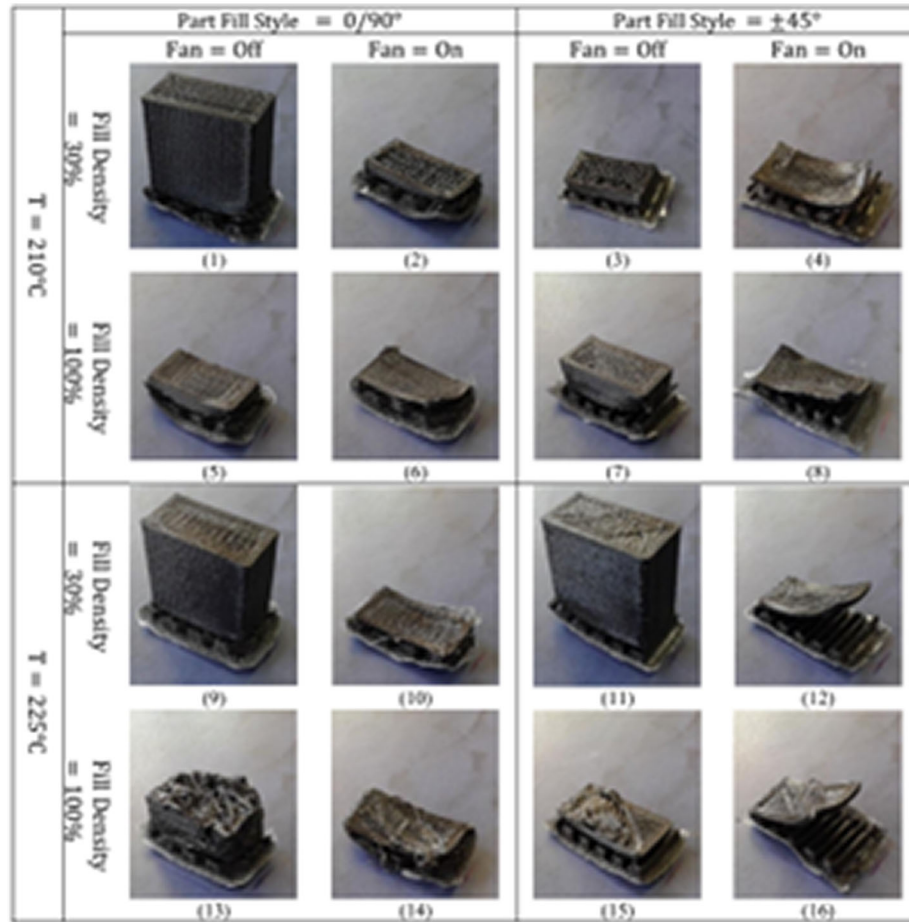
Figure 6 shows the first layer of the three directions of the experiment. As can be seen, direction I exhibit higher heat transfer compared to the other directions. Therefore, as there is a higher ΔT , the force created from the decrease in temperature is more intense than in the other two directions. On the other hand, in the direction I, in addition to more decrease in temperature, the layers adhere together. Therefore, the force related to the newer layer affects the older one, consequently weakening the older layer's attachment, and finally resulting in the detachment of the last layer from the bed. However, heat transfer in directions II and III are the same, and there is no interaction between the layers as they shrink independently. The results of the other experiment also confirm this observation that directions II and III show superior performance over the direction I. Among directions II and III, direction III displays better results because the layers are not suddenly deposited on the support. In direction II, a layer of semi-crystalline polymer material is deposited on the surface. The shrinkage of this layer ruins the support and fails the printing process. However, in direction III, there is a gradual increase in the volume of the layers.

5.2 Printing Direction II

Under this printing direction, three sample items made of semi-crystalline polymers are printed under 30% filling percentage when the fan mode is off. Therefore, it can be concluded that turning the fan on leads to an increase in shrinkage and detachment of the layers from the bed as there is an increase in ΔT and filling percentage. The filling percentage increases because of the increase in the volume of the material required for printing. The three printed samples are presented in Fig. 7. The shrinkage in the first layers can be clearly observed which is one of the drawbacks of the printing parts in this direction. It is found that the shrinkage under 225 °C and ± 45 direction (Experiment 11) is more than the similar sample with 0/90 printing direction. This point reveals that the tool's path also affects the shrinkage, and the ± 45 direction yields a



(a)



(b)

Fig. 4 Printed samples with (a) printing direction I, (b) printing direction II and (c) printing direction III

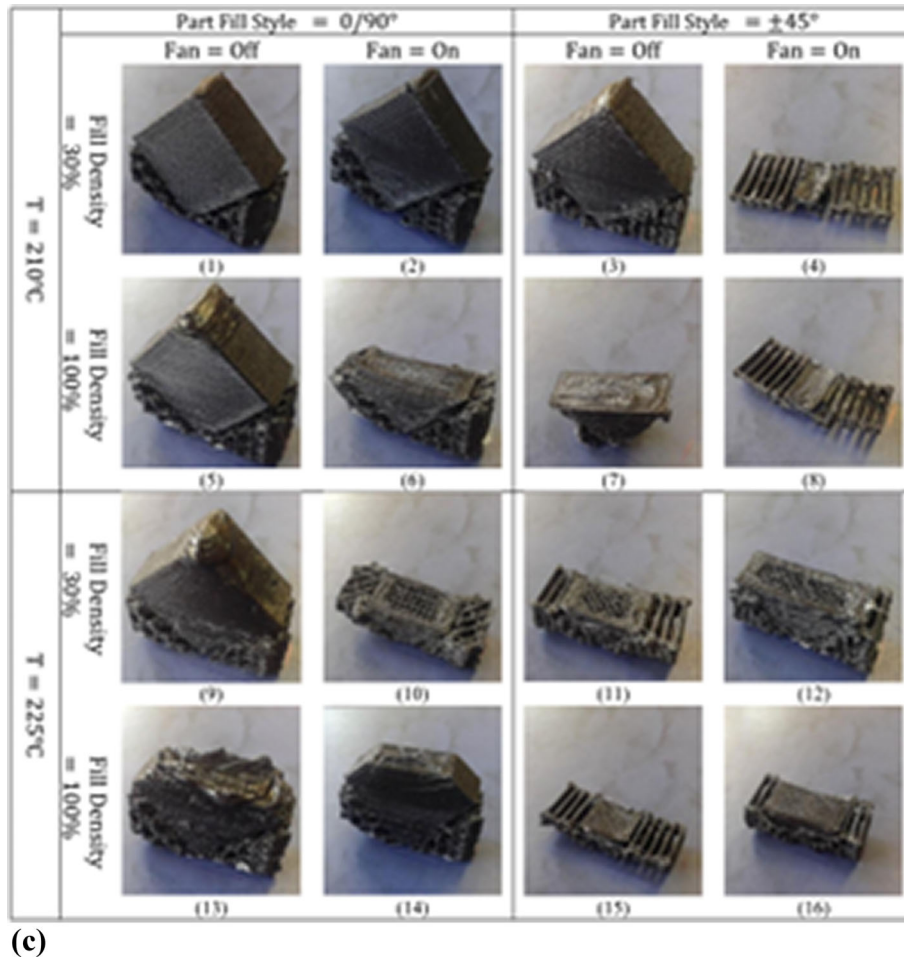


Fig. 4 continued

higher shrinkage. This result can be extracted from the comparison of the first and second columns of Fig. 4(b) with the third and fourth columns of Fig. 4(b), respectively. Another defect in the printed part with direction II is the very high surface roughness of the bottom of the part (the first layer of the part) in which, in addition to the effect of the support on it, the rasters are separated from each other due to high shrinkage in this layer (Fig. 7b).

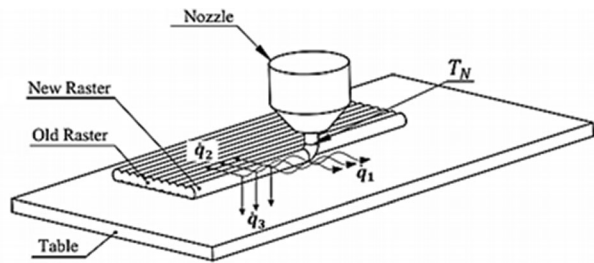
5.3 Printing Direction III

Five sample items are printed with the printing direction III which is the best condition for printing of semi-crystalline parts. The results under this direction were similar to the results from direction II. Fan off mode, 0/90 filling pattern, and a lower filling percentage facilitate the printing process. By comparing the first eight experiments with the second eight experiments (Fig. 4c), it can be concluded that the increase in temperature is not advantageous to printing semi-crystalline parts since an increase in temperature leads to an increase in ΔT and according to Eq 5, increases the force related to the layer's shrinkage. Therefore, the printing process gets cumbersome. Another drawback of the increase in temperature is deterioration in the surface roughness of the object at the region where it attaches to the support (Fig. 8a). This happens as a result of the decrease in viscosity of the semi-crystalline materials with an increase in temperature. When the nozzle moves from the left

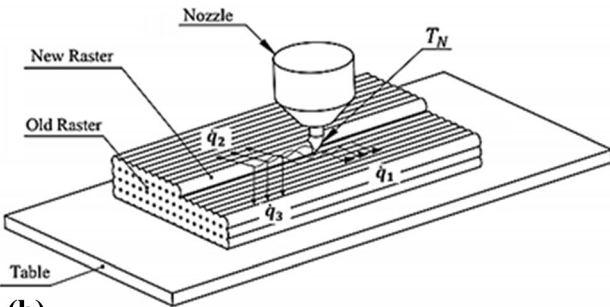
support to the right one to deposit the layers, due to the low viscosity of the material, the layer does not detach from the nozzle tip and stretches over the surface of the object. This leads to deterioration in the surface of the object. This drawback can be avoided by modifying the nozzle's path. It should be noted that at low temperatures (Experiments 1 to 3 and 5 in Fig. 4c), this issue does not exist.

Two other faults also can be found in the printed objects, i.e., delamination and molten pool (Fig. 8b, c). The delamination occurs by turning the fan on, and the molten pool (in the upper section of the part) is created when the fan is off. Delamination occurs due to the cooling effect of the fan, when the layers' shrinkage forces surpass the adhesion force between adjacent layers, and they get separated from each other. On the other hand, the fan off mode and a decrease in the cross-sectional area of printing lead to the deposition of excessive material on the layers, and due to the lack of enough time for solidification, the molten pool are created. However, with an efficient cooling system, molten pools will be avoided. Therefore, to remove the molten pools, the fan must be on, and to avoid delamination, the velocity of the fan must be controlled.

In Fig. 9, the item is printed under the controlled velocity of the fan. In this case, the fan is turned on for the last layers and gradually its velocity is increased until the last layer which the fan was under full load operation (Fig. 9b). As can be seen, the part is printed without any faults such as delamination, molten



(a)



(b)

Fig. 5 Heat transfer in rasters: (a) first layer and (b) next layer

pool, and deterioration in surface roughness at the support region. It should be noted that under this printing direction, there is no sign of the rough surface and contraction in the first layers of the object, which exist with direction II (defects in Fig. 7).

The dimensions of the final printed part (Fig. 9) are given in Table 3. The dimensions of length, width, and height are the average dimension of four different points of the piece. As can be seen, the maximum error is 1.42% in the length and height of the piece.

6. Evaluating the Mechanical Properties of the Printed Samples

After investigating how it is possible to print semi-crystalline parts with a very high shrinkage percentage, the mechanical properties of the printed samples can be evaluated. All samples are printed with optimal conditions as shown in Fig. 9. The maximum tensile strength, flexural strength, and compression strength are equal to 11.5 ± 1.1 , 28 ± 2.3 , and 8 ± 1.7 MPa, respectively. The reason for the low tensile strength compared to the previous literature (Ref 38) is that with the direction of printing, the rasters are not aligned with the load and the low tensile strength is obtained. The direction of the rasters in other tests did not have much effect and the

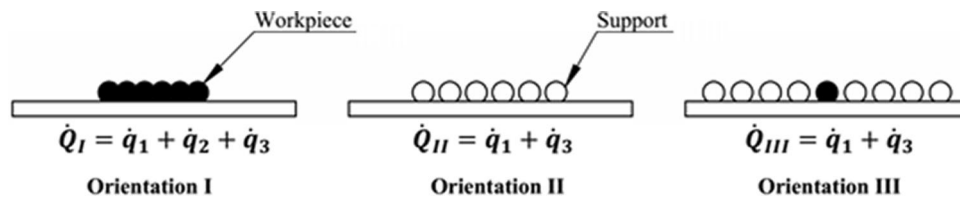


Fig. 6 Heat transfer in the printing direction of the part: (a) Printing direction I, (b) Printing direction II, and (c) Printing direction III

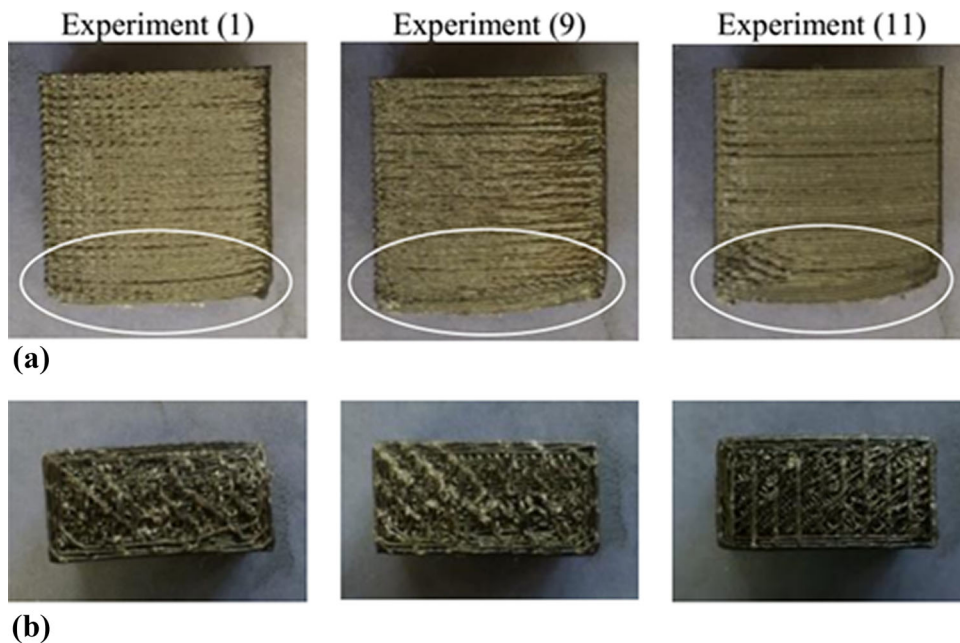


Fig. 7 Defects created in the printed part with direction II: (a) shrinkage in the primary layers and (b) low-quality surface finish of the first layer (subsurface of the part)

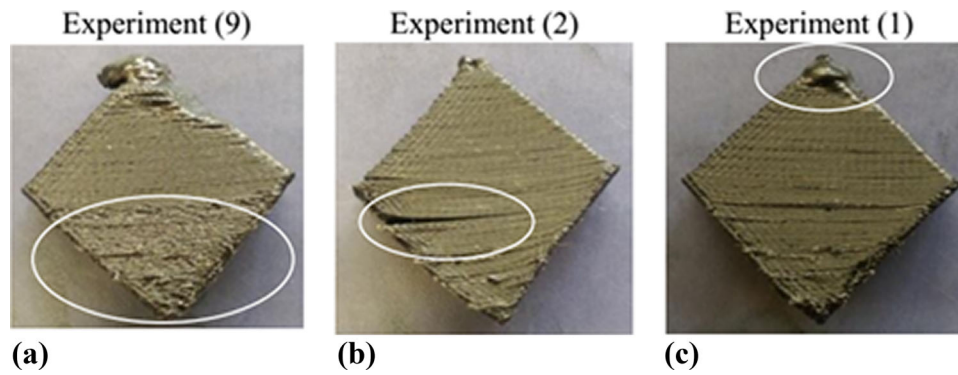


Fig. 8 Defects in the printed parts with direction III: (a) inappropriate surface smoothness at high temperature, (b) delamination of the part with the fan on mode, and (c) molten pool with the fan off mode

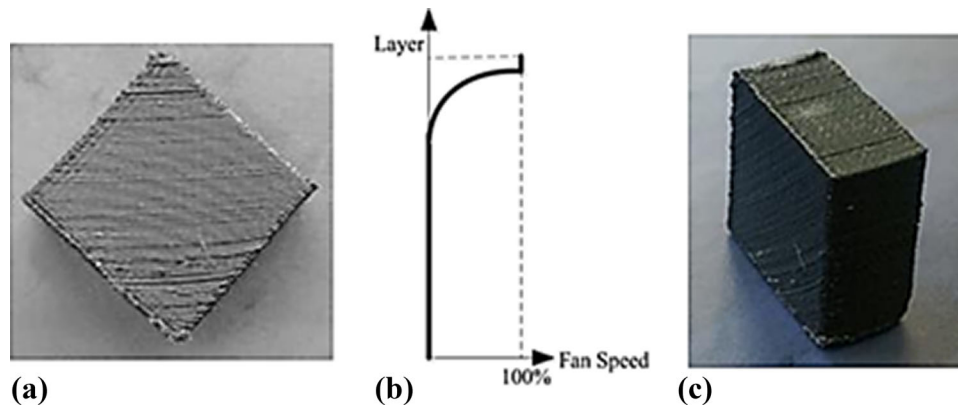


Fig. 9 Printing of a semi-crystalline part with optimal conditions: (a) printing direction, (b) fan speed increase curve, and (c) printed part

obtained values are consistent with the results obtained in the previous literature.

7. Conclusion

Printing parts from semi-crystalline materials using the FFF method is difficult due to the high shrinkage that they exhibit as compared to amorphous polymers. Therefore, this study aims at investigating the printing of these materials. The printing direction is one of the critical parameters that affect the printing process of these materials. With proper printing direction, it is possible to print semi-crystalline parts. In this paper, three different directions are studied, and under each direction, various parameters such as the temperature of the nozzle, the fan mode, the filling percentage, and the filling pattern are investigated. To investigate the printing direction, the parts are printed on the bed (direction I), support (direction II), and smallest edge of the object (direction III). It is observed that any part can be printed in the first direction as a result of the high shrinkage force in layers. Under the second direction, three samples are printed, and all of them suffer from the high surface roughness and high shrinkage in the first layers. The parts that are printed under the third direction suffer from faults such as delamination, molten pool, and deterioration in the surface roughness. Nevertheless, under this direction, with proper modification of the process parameters, the flawless semi-crystalline part is printed. The maximum dimensional error for

this printed object is 1.41% along its length. Under all three printing directions, the fan off mode, 0/90 filling pattern and low filling percentage facilitate the printing process of the semi-crystalline object.

Funding

The author(s) received no financial support for the research, authorship, and/or publication of this article.

Conflict of interest

The author(s) declared no potential conflicts of interest with respect to the research, authorship, and/or publication of this article.

References

1. Kumar J, Mishra V, and Negi S (2022) An Overview of Research on FFF Based Additive Manufacturing of Polymer Compositet
2. M.N.M. Norani, M.I.H.C. Abdullah, M.F.B. Abdollah, H. Amiruddin, F.R. Ramli, N. Tamaldin, D. Tunggai, F.T.K.M. dan Pembuatan, and U.T. Malaysia, Mechanical and Tribological Properties of FFF 3D-printed Polymers: A Brief Review, *J. Tribol.*, 2021, **29**, p 11–30
3. S. Abidaryan, B. Akhouni, and F. Hajami, Additive Manufacturing and Investigation of Shape Memory Properties of Poly(lactic Acid)/Thermoplastic Polyurethane Blend, *J Elastomers Plast*, 2021 <https://doi.org/10.1177/00952443221147028>

4. B. Akhouni and F. Hajami, Extruded Polymer Instability Study of the Polylactic Acid in Fused Filament Fabrication Process: Printing Speed Effects on Tensile Strength, *Polym. Eng. Sci.*, 2022, **62**(12), p 4145–4155. <https://doi.org/10.1002/pen.26174>
5. L.J. Tan, W. Zhu, and K. Zhou, Recent Progress on Polymer Materials for Additive Manufacturing, *Adv. Func. Mater.*, 2020, **30**(43), p 2003062
6. S. Wickramasinghe, T. Do, and P. Tran, FDM-Based 3D Printing of Polymer and Associated Composite: A Review on Mechanical Properties, Defects and Treatments, *Polymers*, 2020, **12**(7), p 1529
7. N.G. Tanikella, B. Wittbrodt, and J.M. Pearce, Tensile Strength of Commercial Polymer Materials for Fused Filament Fabrication 3D Printing, *Addit. Manuf.*, 2017, **15**, p 40–47
8. O.S. Carneiro, A. Silva, and R. Gomes, Fused deposition modeling with polypropylene, *Mater. Des.*, 2015, **83**, p 768–776
9. M. Rinaldi, T. Ghidini, F. Cecchini, A. Brandao, and F. Nanni, Additive Layer Manufacturing of Poly (Ether Ether Ketone) via FDM, *Compos. B Eng.*, 2018, **145**, p 162–172
10. Bagsik A, Schöppner V, Klemp E *FDM Part Quality Manufactured with Ultem* 9085*. In: 14th International Scientific Conference on Polymeric Materials, 2010, p 307–315
11. B. Akhouni, A.H. Behraves, and A. Bagheri Saed, An Innovative Design Approach in Three-Dimensional Printing of Continuous Fiber-Reinforced Thermoplastic Composites via Fused Deposition Modeling Process: In-melt Simultaneous Impregnation, *Proc. Inst. Mech. Eng. Part B J. Eng. Manuf.*, 2020, **234**(1–2), p 243–259
12. D. Zhu, Y. Ren, G. Liao, S. Jiang, F. Liu, J. Guo, and G. Xu, Thermal and Mechanical Properties of Polyamide 12/Graphene Nanoplatelets Nanocomposites and Parts Fabricated by Fused Deposition Modeling, *J. Appl. Polym. Sci.*, 2017, **134**(39), p 45332
13. M. Nabipour, A.H. Behraves, and B. Akhouni, Effect of Printing Parameters on Mechanical Strength of Polymer-Metal composites Printed via FDM 3D Printer, *Modares Mech. Eng.*, 2017, **17**(1), p 145–150
14. D. Espalin, K. Arcaute, D. Rodriguez, F. Medina, M. Posner, and R. Wicker, Fused Deposition Modeling of Patient-Specific Polymethylmethacrylate Implants, *Rapid Prototyping J.*, 2010, **16**, p 164–173
15. S.K. Hedayati, A.H. Behraves, S. Hasannia, A.B. Saed, and B. Akhouni, 3D Printed PCL Scaffold Reinforced with Continuous Biodegradable Fiber Yarn: A Study on Mechanical and Cell Viability Properties, *Polym. Testing*, 2020, **83**, 106347
16. Z. Quan, J. Suhr, J. Yu, X. Qin, C. Cotton, M. Mirotznik, and T.-W. Chou, Printing Direction Dependence of Mechanical Behavior of Additively Manufactured 3D Preforms and Composites, *Compos. Struct.*, 2018, **184**, p 917–923
17. T.A. Osswald and G. Menges, *Materials Science of Polymers for Engineers*, Carl Hanser Verlag GmbH Co KG, Germany, 2012
18. B.S. Solanki, H. Singh, and T. Sheorey, Effect of Injection Molding Cycle Time on Shrinkage and Weight of Manufactured Polymer Gear, *Mater Today Proc.*, 2022, **62**, p A1–A6
19. T.-M. Wang, J.-T. Xi, and Y. Jin, A Model Research for Prototype Warp Deformation in the FDM Process, *Int. J. Adv. Manuf. Technol.*, 2007, **33**(11), p 1087–1096
20. B. Akhouni and A.H. Behraves, Effect of Filling Pattern on the Tensile and Flexural Mechanical Properties of FDM 3D Printed Products, *Exp. Mech.*, 2019, **59**(6), p 883–897
21. K. Rajan, M. Samykano, K. Kadirgama, W.S.W. Harun, and M. Rahman, Fused Deposition Modeling: Process, Materials, Parameters, Properties, and Applications, *Int. J. Adv. Manuf. Technol.*, 2022, **120**, p 1531–1570
22. A. Sola, Materials Requirements in Fused Filament Fabrication: A Framework for the Design of Next-Generation 3D Printable Thermoplastics and Composites, *Macromol. Mater. Eng.*, 2022, **307**, p 2200197
23. B. Akhouni, A.H. Behraves, and A. Bagheri Saed, Improving Mechanical Properties of Continuous Fiber-Reinforced Thermoplastic Composites Produced by FDM 3D Printer, *J. Reinf. Plast. Compos.*, 2019, **38**(3), p 99–116
24. M. Nabipour and B. Akhouni, An Experimental Study of FDM Parameters Effects on Tensile Strength, Density, and Production Time of ABS/Cu Composites, *J. Elastomers Plast.*, 2021, **53**(2), p 146–164
25. M. Nabipour, B. Akhouni, and A. Bagheri Saed, Manufacturing of Polymer/Metal Composites by Fused Deposition Modeling Process with Polyethylene, *J. Appl. Polym. Sci.*, 2020, **137**(21), p 48717
26. L. Yang, S. Li, X. Zhou, J. Liu, Y. Li, M. Yang, Q. Yuan, and W. Zhang, Effects of Carbon Nanotube on the Thermal, Mechanical, and Electrical Properties of PLA/CNT Printed Parts in the FDM Process, *Synth. Met.*, 2019, **253**, p 122–130
27. V.C. Gavali, P.R. Kubade, and H.B. Kulkarni, Mechanical and Thermo-Mechanical Properties of Carbon Fiber Reinforced Thermoplastic Composite Fabricated Using Fused Deposition Modeling Method, *Mater. Today Proc.*, 2020, **22**, p 1786–1795
28. W. Peng, Z. Bin, D. Shouling, L. Lei, and C. Huang, Effects of FDM-3D Printing Parameters on Mechanical Properties and Microstructure of CF/PEEK and GF/PEEK, *Chin. J. Aeronaut.*, 2021, **34**(9), p 236–246
29. B. Akhouni, M. Nabipour, F. Hajami, and D. Shakoori, An Experimental Study of Nozzle Temperature and Heat Treatment (Annealing) Effects on Mechanical Properties of High-temperature Polylactic Acid in Fused Deposition Modeling, *Polym. Eng. Sci.*, 2020, **60**(5), p 979–987
30. B. Maidin, M. Muhamad, E. Pei, Feasibility Study of Ultrasonic Frequency Application on fdm to Improve Parts Surface Finish. *J. Technol.*, 2015, **77**(32)
31. W. Wu, J. Jiang, H. Jiang, W. Liu, G. Li, B. Wang, M. Tang, and J. Zhao, Improving Bending and Dynamic Mechanics Performance of 3D Printing Through Ultrasonic Strengthening, *Mater. Lett.*, 2018, **220**, p 317–320
32. P. Wang and B. Zou, Improvement of Heat Treatment Process on Mechanical Properties of FDM 3D-Printed Short-and Continuous-Fiber-Reinforced PEEK Composites, *Coatings*, 2022, **12**(6), p 827
33. H. Zhao, X. Liu, W. Zhao, G. Wang, and B. Liu, An Overview of Research on FDM 3D Printing Process of Continuous Fiber Reinforced Composites, *J. Phys. Conf. Ser.*, 2019, **5**, p 052037
34. B. Akhouni, M. Nabipour, F. Hajami, S.S. Band, and A. Mosavi, Calculating Filament Feed in the Fused Deposition Modeling Process to Correctly Print Continuous Fiber Composites in Curved Paths, *Materials*, 2020, **13**(20), p 4480
35. B. Akhouni, M. Nabipour, O. Kordi, and F. Hajami, Calculating Printing Speed in Order to Correctly Print PLA/Continuous Glass Fiber Composites via Fused Filament Fabrication 3D Printer, *J. Thermoplast. Compos. Mater.*, 2021, **36**, p 162–181
36. Z. Zhang and X. Gao, Polypropylene Random Copolymer Based Composite Used for Fused Filament Fabrication: Printability and Properties, *Polymers*, 2022, **14**(6), p 1106
37. I. Polyakov, G. Vaganov, A. Didenko, E. Ivan'kova, E. Popova, Y. Nashchekina, V. Elokhoyskiy, V. Svetlichnyi, and V. Yudin, Development and Processing of New Composite Materials Based on High-Performance Semicrystalline Polyimide for Fused Filament Fabrication (FFF) and Their Biocompatibility, *Polymers*, 2022, **14**(18), p 3803
38. Tian P (2020) Additive Manufacturing and Characterization of Polyoxymethylene
39. I. Muro-Fraguas, E. Sainz-García, A. Pernía-Espinoza, and F. Alba-Eliás, Atmospheric Pressure Air Plasma Treatment to Improve the 3D Printing of Polyoxymethylene, *Plasma Processes Polym.*, 2019, **16**(7), p e1900020
40. Y.-T. Wang, Y.-T. Yeh, Effect of print angle on mechanical properties of FDM 3D structures printed with POM material. In: *Innovative Design and Development Practices in Aerospace and Automotive Engineering*. Springer, (2017), p 157–167
41. S. Lebedev, O. Gefle, E. Amitov, D. Zhuravlev, and D.Y. Berchuk, Thermophysical, Rheological and Morphological Properties of Polyoxymethylene Polymer Composite for Additive Technologies, *Russ. Phys. J.*, 2018, **61**(6), p 1029–1033
42. A. Antony Samy, A. Golbang, E. Harkin-Jones, E. Archer, M. Dahale, and A. McIlhagger, Influence of Ambient Temperature on Part Distortion: A Simulation Study on Amorphous and Semi-Crystalline Polymer, *Polymers*, 2022, **14**(5), p 879
43. M. Golzar, J. Sinke, and M. Abouhamzeh, Novel Thermomechanical Characterization for Shrinkage Evolution of Unidirectional Semicrystalline Thermoplastic Prepregs (PPS/CF) in Melt, Rubbery and Glassy States, *Compos. A Appl. Sci. Manuf.*, 2022, **156**, p 106879
44. N. Omar, N. Shuaib, M. Ab Hadi, and A. Azmi, Mechanical Properties of Carbon and Glass Fibre Reinforced Composites Produced by Additive Manufacturing: A Short Review, *IOP Conf. Ser. Mater. Sci. Eng.*, 2019, **1**, p 012020
45. J.P. Holman, *Heat Transfer*, McGraw Hill Higher Education, New York, 2010

46. F.P. Beer, E.R. Johnston, J.T. DeWolf, and D.F. Mazurek, *Statics and Mechanics of Materials*, McGraw-Hill Education, New York, 2017

Publisher's Note Springer Nature remains neutral with regard to jurisdictional claims in published maps and institutional affiliations.

Springer Nature or its licensor (e.g. a society or other partner) holds exclusive rights to this article under a publishing agreement with the author(s) or other rightsholder(s); author self-archiving of the accepted manuscript version of this article is solely governed by the terms of such publishing agreement and applicable law.